

EVLM: Self-Reflective Multimodal Reasoning and KTO Alignment for Cross-Dimensional Visual Editing

Umar Khalid^{1*}, Kashif Munir^{1*}, Hasan Iqbal², Azib Farooq³, Jing Hua², Nazanin Rahnavard⁴,
Chen Chen⁴, Victor Zhu¹, Zhengping Ji¹

¹Axon, USA

²Wayne State University, USA

³Miami University, USA

⁴University of Central Florida, USA

ukhalid@axon.com, kmunir@axon.com, hasan.iqbal1292@gmail.com,

azibfarooq10@gmail.com,

jinghua@wayne.edu, nazanin.rahnavard@ucf.edu, chen.chen@crcv.ucf.edu,

vzhu@axon.com, zji@axon.com

Abstract

Editing complex visual content from ambiguous or partially specified instructions remains a core challenge in vision–language modeling. Existing models can contextualize content but often fail to infer the **underlying intent** within a reference image or scene, leading to inconsistent or misaligned edits. We introduce the Editing Vision–Language Model (EVLM), a system that interprets ambiguous instructions in conjunction with reference visuals to produce precise, context-aware editing prompts. EVLM’s key innovation is a reflective reasoning framework that translates subjective user intent into structured, actionable outputs by aligning with human-rated rationales through Reflection-Aware KL-Divergence Target Optimization (RKTO). By combining Chain-of-Thought (CoT) reasoning with RKTO alignment, EVLM captures fine-grained editing preferences without relying on binary supervision. Trained on a dataset of 30,000 CoT examples with human-annotated rationale quality, EVLM achieves substantial gains in alignment with human intent. Experiments across image, video, 3D, and 4D editing tasks show that EVLM generates coherent and high-quality instructions, providing a scalable foundation for multimodal editing and reasoning.

Introduction

Recent advances in text-to-image (T2I) diffusion models have enabled free-form natural language to be transformed into photorealistic imagery with striking fidelity (Ramesh et al. 2021; Ho et al. 2022; Rombach et al. 2022). Building on this progress, instruction-based editors—“*modify this image according to that sentence*”—have become a natural interface for visual content creation (Brooks, Holynski, and Efros 2023; Kawar et al. 2023; Zhang and Agrawala 2023). However, as editing tasks become more open-ended and multimodal—combining vague language with incomplete visual cues—current systems often fail to interpret user intent. This raises a central challenge for multimodal reasoning: *can a*



Figure 1: Reference image and prompt for the 3D editing task: “An Einstein Face!” The reference includes an image with a mustache and the image-with-text “Green Jacket.” These were provided to GPT-4o, along with supporting prompts (details in *supplementary*), to guide the generation of accurate editing instructions. GPT-4o encountered challenges integrating textual, visual, and OCR information to produce coherent instructions. Despite multiple attempts, DALL-E 3 guided by GPT-4o was unable to generate the desired edited image that fully aligns with the *reference intent*.

model reason through ambiguity, reconciling partial textual hints with reference visuals to infer the user’s intended edit?

Motivation. Prompt-refinement pipelines that attach a large language model to a diffusion decoder (Ge et al. 2024; Zhao et al. 2024) perform well when instructions are explicit but lack *reflective reasoning*. Given an instruction such as “*Give it an Einstein face!*” with only weak visual hints (Fig. 1), these systems cannot justify *why* a specific region—such as the jacket—should inherit a pattern or texture. Two factors contribute to this limitation: (i) existing datasets contain only terse text–edit pairs, providing no supervision for reasoning, and (ii) preference optimization with PPO (Schulman et al. 2017) captures only coarse binary rewards, which are unsuited for subjective, multi-solution editing tasks where subtle human preferences matter.

We introduce the **Editing Vision–Language Model (EVLM)**, a multimodal reasoning framework that interprets ambiguous editing instructions by combining textual, visual,

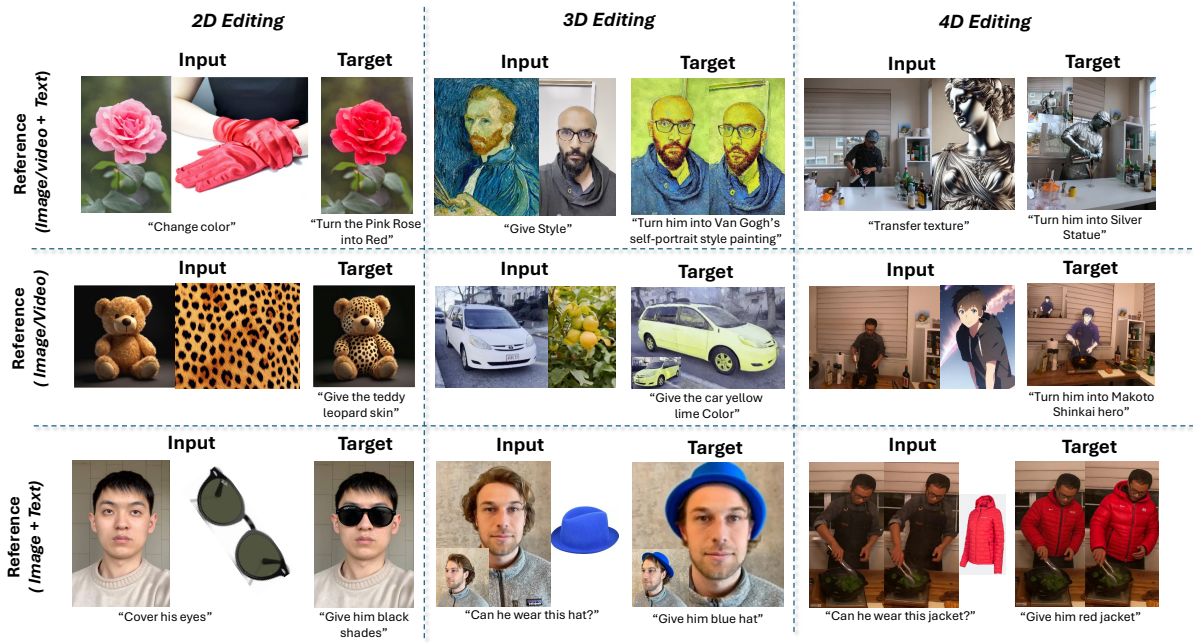


Figure 2: EVLM enables editing across 2D, 3D, and 4D tasks. Given a reference image, video, or text instruction, EVLM generates precise and context-aware editing transformations. Examples include color and style modifications in 2D and 3D, and texture or dynamic edits in 4D scenarios. These results highlight EVLM’s multimodal understanding of spatial, temporal, and semantic cues for complex visual editing.

and spatial cues. EVLM ingests diverse references—such as images, video clips, depth maps, or text—and outputs concise, disambiguated instructions together with target masks or object indices suitable for downstream visual editors.

Training proceeds in two complementary stages: (1) construction of the **REFLECTIVE-EDIT** dataset of 30k multimodal examples, where GPT-4o generates chain-of-thought rationales that are rated by human annotators as *desired* or *non-desired*; and (2) alternating phases of *Reflective Supervised Fine-Tuning* (SFT) and **Reflection-Aware KL-Divergence Target Optimization** (RKTO), which align both the final instructions and the reflective reasoning process with human preferences. Together, these components enable EVLM not only to imitate editing instructions but also to reason reflectively about user intent with interpretable internal logic as illustrated in Fig. 2. Our main contributions are:

1. **EVLM**, a vision–language model capable of reflective multimodal reasoning for context-aware and interpretable editing across image, video, 3D, and 4D domains.
2. **REFLECTIVE-EDIT**, a 30k-example chain-of-thought dataset with human preference annotations designed to teach reflective reasoning for editing tasks.
3. **RKTO**, a preference-alignment framework that extends KL-divergence target optimization to jointly align instruction effectiveness and reflection quality, providing richer and more stable feedback than PPO-based methods.

Related Work

Reflection and Alignment in Multimodal Models. Recent work explores reflection in language and vision-language models

to enable post-hoc self-correction and alignment with human intent. Methods use either external feedback (*e.g.*, execution traces, expert critiques) (Shinn et al. 2023; Chen et al. 2024a) or internal self-evaluation (Madaan et al. 2024; Li, Yang, and Ettinger 2024; Weng et al. 2023), though reliability remains task-dependent (Huang et al. 2023). Parallel efforts in vision-language models apply chain-of-thought reasoning to domains such as math (Lu et al. 2023; Wang et al. 2024a), scientific QA (Lu et al. 2022), and chart understanding (Zhang et al. 2024). Preference-alignment approaches like DPO (Ouali et al. 2024; Sun et al. 2023) and PPO (Yu et al. 2024) guide model fine-tuning, while iterative DPO (Sun et al. 2024; Pang et al. 2024) improves step-by-step reasoning. More recently, KTO (Ethayarajh et al. 2024) aligns model outputs to a soft reference distribution via KL-divergence, effectively modeling nuanced human preferences for subjective generation tasks such as visual editing.

Diffusion-Based Editing Across Dimensions. Diffusion-based models enable text-driven editing across modalities, spanning 2D (Ruiz et al. 2023; Tumanyan et al. 2022; Hertz et al. 2022; Meng et al. 2021; Brooks, Holynski, and Efros 2023), 3D (Kamata et al. 2023; Haque et al. 2023a; Dong and Wang 2024), and 4D (Zhuang et al. 2023; Shao et al. 2023) domains. Extensions to videos include Tune-A-Video (Wu et al. 2023), Make-A-Video (Singer et al. 2023), and MagicVideo (Zhou et al. 2022), which leverage spatio-temporal attention to maintain consistency. Prompt-level control methods such as Prompt-to-Prompt (Hertz et al. 2022) and Plug-and-Play (Tumanyan et al. 2022) refine local edits, while 3D and 4D variants adapt text-to-image priors (*e.g.*, IP2P) for NeRFs and dynamic scenes. Our work builds on these foundations by integrating reflective reasoning and alignment into the diffusion pipeline, yielding flexible editing across 2D, 3D, and 4D modalities.

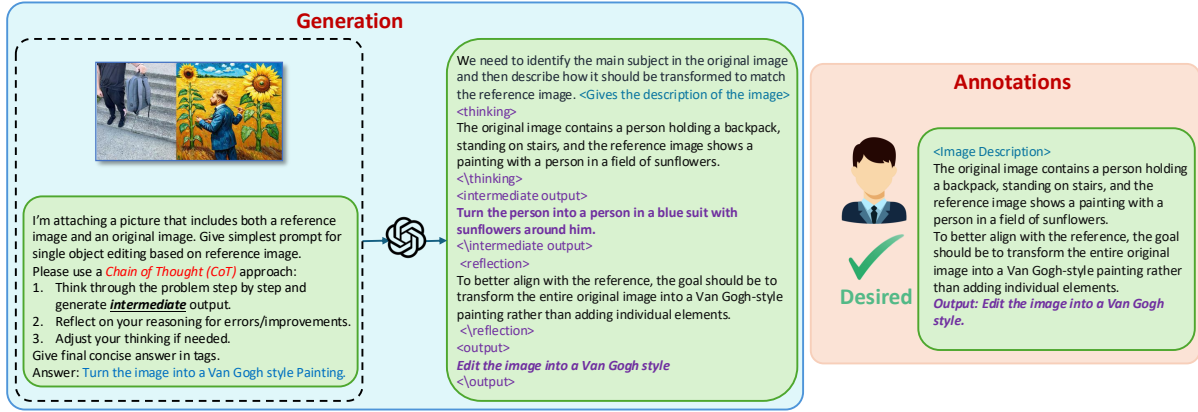


Figure 3: **Overview of our data preparation pipeline.** Given a reference and target image, GPT-4o produces a structured chain-of-thought rationale through initial, intermediate, and reflective reasoning. Only the reflective and final outputs are used to construct RKTO training data, with human annotators providing “desired” labels when reasoning aligns with intended edits.

Approach

The Editing Vision–Language Model (EVLM) converts multimodal editing intent—including images, video, and text—into concise and interpretable editing instructions accompanied by spatial masks. Training proceeds in three stages: (1) construction of a reflective dataset using GPT-4o, (2) supervised fine-tuning (SFT) of a Qwen2-VL-7B backbone for structured reasoning, and (3) reflection-aware KL-Divergence Target Optimization (RKTO) to align both the generated instructions and the underlying reflective reasoning with human preferences. (Notations and full derivations are provided in the Supplementary.)

REFLECTIVE-EDIT Dataset

We construct the REFLECTIVE-EDIT dataset containing approximately 30,000 multimodal examples. Each example contains an input, one or more reference items (image, video, or text), and a GPT-4o-generated chain-of-thought (CoT) trace segmented into `<thinking>`, `<intermediate>`, `<reflection>`, and `<output>` sections. Human annotators label each trace as *desired* or *non-desired*, providing graded preference supervision for both instruction quality and reflective reasoning. Figure 3 summarizes the data-preparation pipeline, including CoT generation and human annotation.

Supervised Fine-Tuning (SFT)

EVLM first learns to reproduce GPT-4o CoT traces using teacher forcing. For a tuple $(\mathcal{V}, u, y_{1:T})$, where \mathcal{V} denotes the visual context, u the textual prompt, and $y_{1:T}$ the target token sequence (which may include mask tokens yielding a discrete mask \hat{m}), the SFT objective is

$$\mathcal{L}_{\text{SFT}} = - \sum_{t=1}^T \log p_{\theta}(y_t | y_{<t, u, \mathcal{V}}),$$

which stabilizes token-level generation and provides the reference snapshot ρ_{ref} used in subsequent alignment. When

available, the dataset also provides a reference mask m_{ref} for downstream evaluation.

Reflection-Aware KTO (RKTO)

We extend KL-Divergence Target Optimization (KTO) by incorporating a reflection reward that encourages concise, consistent reflective reasoning in addition to instruction fidelity. For a tuple $(\mathcal{V}, u, y_{\text{pref}}, m_{\text{ref}})$, the per-sample RKTO objective is

$$\mathcal{L}_{\text{RKTO}} = \mathbb{E} \left[w(s_{\phi} - \eta_0) R_{\text{eff}}(\hat{y}, \hat{m}; y_{\text{pref}}, m_{\text{ref}}) + \lambda_{\text{ref}} R_{\text{reflect}}(r_{\text{ref}}) \right], \quad (1)$$

where

$$s_{\phi} = \log \frac{\rho_{\phi}(y_{\text{pref}} | u, \mathcal{V})}{\rho_{\text{ref}}(y_{\text{pref}} | u, \mathcal{V})}, \quad (2)$$

$$\eta_0 = \text{KL}(\rho_{\phi}(\cdot | u, \mathcal{V}) \parallel \rho_{\text{ref}}(\cdot | u, \mathcal{V})).$$

Here we clarify key terms used above: ρ_{pref} denotes the empirical human-preferred distribution estimated from annotator labels; \hat{m} denotes the model-decoded mask (from mask tokens) and m_{ref} the dataset reference mask; IoU is non-differentiable and is handled via REINFORCE with a batch baseline; $w(\cdot)$ is softplus followed by clipping to $[0, w_{\text{max}}]$; cosine similarities are rescaled to $[0, 1]$ by $\widetilde{\text{cos}}(a, b) = (1 + \cos(a, b))/2$; and r_{ref} denotes the reflection segment from the CoT trace.

Instruction Effectiveness. When a reference mask m_{ref} is available, the instruction-effectiveness reward combines semantic and spatial alignment:

$$R_{\text{eff}}(\hat{y}, \hat{m}; y_{\text{pref}}, m_{\text{ref}}) = \alpha \widetilde{\text{cos}}(e(\hat{y}), e(y_{\text{pref}})) + (1 - \alpha) \text{IoU}(\hat{m}, m_{\text{ref}}), \quad (3)$$

where $e(\cdot)$ is the Qwen2-VL encoder, $\widetilde{\text{cos}}(a, b) = (1 + \cos(a, b))/2$ rescales cosine similarity to $[0, 1]$, and IoU



Figure 4: **Image Editing Results Using Reference Images or Text Prompts.** The first row demonstrates EVLM’s ability to refine vague textual prompts into precise editing instructions and to produce masks for targeted edits. The second row compares EVLM to an image-based editing baseline, illustrating improved alignment to reference-guided transformations.

notes intersection-over-union between predicted and reference masks. IoU is non-differentiable and is optimized via REINFORCE with a batch baseline.

Reflection Reward. The reflection-quality reward is

$$\begin{aligned}
 R_{\text{reflect}}(r_{\text{ref}}) = & \beta_1 \widetilde{\text{cos}}(e(r_{\text{ref}}), e(y_{\text{pref}})) \\
 & + \beta_2 \exp(-\gamma \text{len}(r_{\text{ref}})) \\
 & + \beta_3 (1 - \text{KL}(p_{\text{int}} \| p_{\text{ref}})),
 \end{aligned}$$

where p_{int} and p_{ref} are predictive token distributions for the `<intermediate>` and `<reflection>` segments, and the β coefficients sum to one. The reflection loss is $\mathcal{L}_{\text{reflect}} = 1 - R_{\text{reflect}}$.

Gradient Estimation and Optimization

RKTO computes gradients at the sequence level, combining differentiable token-likelihood terms with policy gradients for non-differentiable components such as IoU. For a batch of B preference examples, the weighted objective involves normalized log-ratio and baseline statistics given by

$$s_\phi = \log \frac{\rho_\phi(y_{\text{pref}} | u, \mathcal{V})}{\rho_{\text{ref}}(y_{\text{pref}} | u, \mathcal{V})}, \quad (4)$$

$$\eta_0 = \text{KL}(\rho_\phi(\cdot | u, \mathcal{V}) \parallel \rho_{\text{ref}}(\cdot | u, \mathcal{V})).$$

The instruction-effectiveness reward, which combines semantic and spatial consistency, is formulated as

$$\begin{aligned}
 R_{\text{eff}}(\hat{y}, \hat{m}; y_{\text{pref}}, m_{\text{ref}}) = & \alpha \widetilde{\text{cos}}(e(\hat{y}), e(y_{\text{pref}})) \\
 & + (1 - \alpha) \text{IoU}(\hat{m}, m_{\text{ref}}),
 \end{aligned} \quad (5)$$

where $\widetilde{\text{cos}}(a, b) = (1 + \cos(a, b))/2$ rescales the cosine similarity to $[0, 1]$, $e(\cdot)$ is the text-encoder embedding, and IoU is the intersection-over-union between predicted and reference masks.

For conciseness, let

$$c_i = w(\hat{s}_\phi^{(i)} - \hat{\eta}_0), \quad d_i = c_i(1 - \alpha)(\text{IoU}^{(i)} - b_{\text{IoU}}),$$

where b_{IoU} denotes a batch baseline. The resulting gradient estimator can then be expressed as

$$\begin{aligned}
 \nabla_\phi \mathcal{L}_{\text{RKTO}} \approx & \frac{1}{B} \sum_{i=1}^B c_i R_{\text{eff}}^{(i)} \nabla_\phi \log \rho_\phi(y_{\text{pref}}^{(i)} | x^{(i)}) \\
 & + \lambda_{\text{ref}} \nabla_\phi \mathcal{L}_{\text{reflect}} \\
 & + \frac{1}{B} \sum_{i=1}^B d_i \nabla_\phi \log \rho_\phi(\hat{m}^{(i)} | x^{(i)}).
 \end{aligned} \quad (6)$$

The first term represents the importance-weighted policy gradient for the preferred textual response, the second corresponds to the differentiable reflection component, and the third applies a REINFORCE correction for the non-differentiable IoU reward on discrete masks. Variance is reduced through clipping of $w(\cdot)$ to $[0, w_{\text{max}}]$, centering of rewards using batch baselines, and a smaller learning rate for RKTO relative to SFT.

SFT and RKTO are alternated during training. SFT provides a stable reference policy and structured reasoning capacity, while RKTO progressively aligns the model with human-preferred outputs and reflective reasoning. Convergence is observed once validation accuracy and reflection-quality metrics stabilize.

Optimizing Eq. 1 jointly reduces the divergence between the model and human-preferred distributions for both outputs and reflections. Under standard regularity conditions—bounded rewards, monotonic $w(\cdot)$, and sufficiently small learning steps—gradient updates that minimize the RKTO objective also decrease a composite KL divergence between model and preference distributions (see Supplementary for the formal theorem and proof).

Experiments

Model Architecture

Our model builds on the Qwen2-VL-7B architecture (Wang et al. 2024b), which combines a 675M-parameter vision encoder with a 7.6B-parameter language model to strengthen

Table 1: Accuracy comparison across different evaluators on the REFLECTIVE-EDIT benchmark. The last column shows the average accuracy across all evaluators.

Model	Gemini Pro 1.5	LLAMA 405B	GPT-4o	Claude 3.5 Sonnet	Human Evaluators	Avg. Accuracy
mPLUG-Owl (Ye et al. 2023)	44.8	45.1	43.3	42.7	49.0	44.8
mPLUG-Owl2 (Ye et al. 2024)	50.2	51.6	51.3	49.5	51.2	50.8
LLAVA (Liu et al. 2024)	48.3	46.8	47.2	45.9	43.5	46.3
MiniGPT-4 (Zhu et al. 2023)	43.7	44.1	42.5	45.3	47.6	44.6
CogVLM (Wang et al. 2023)	41.4	42.2	40.7	39.6	55.2	43.8
InstructBLIP (Dai et al. 2023)	47.6	46.9	48.4	47.2	56.3	49.2
Qwen-VL (Bai et al. 2023)	49.3	50.4	48.6	47.8	52.4	49.7
LLAMA-3.2-11B (Dubey et al. 2024)	55.5	57.2	56.3	54.8	60.1	56.7
LLAMA-3.2-90B (Dubey et al. 2024)	64.7	63.5	66.1	64.3	58.9	63.5
EVLM-RKTO	95.4	94.8	96.2	95.1	94.1	95.1

multimodal reasoning. Naive Dynamic Resolution (Dehghani et al. 2024) allows variable-size visual inputs by dynamically tokenizing images without absolute position embeddings. We further incorporate 2D-RoPE and Multimodal Rotary Position Embedding (M-RoPE) (Wang et al. 2024b) to encode spatial and temporal relations across text, images, and video, enabling precise positional reasoning.

Evaluation on REFLECTIVE-EDIT

Since generating editing instructions is inherently subjective and often depends on human preferences, we evaluate EVLM using two complementary criteria.

- Human-labeled Evaluation.** We generate editing instructions and ask human annotators to assign binary YES/NO labels, indicating whether the generated instruction semantically aligns with the intended edit. These labels serve as the ground truth for evaluating EVLM and comparing it against other baselines.
- LLM-based Evaluation.** To further ensure scalability and consistency, we employ large language models (LLMs) as automated judges. Specifically, we use four evaluators—Gemini Pro 1.5, LLaMA 405B, GPT-4o, and Claude 3.5 Sonnet—to provide binary YES/NO judgments on 3,000 unseen examples from the REFLECTIVE-EDIT benchmark. Each evaluator marks YES if the generated instruction semantically matches the human reference.

As reported in Table 1, EVLM-RKTO outperforms all

Table 2: Cross-benchmark performance (%) on multimodal reasoning and visual question answering benchmarks.

Benchmark	LLAMA 11B	Qwen2 7B	LLAVA 1.6 (Vicuna 7B)	EVLM (RKTO)
MMMU (val, CoT)	50.7	54.1	35.8	53.0
MMMU-Pro (Vision)	33.0	43.5	–	43.8
MathVista (testmini)	51.5	58.2	34.6	59.1
ChartQA (test, CoT)	83.4	83.0	–	82.8
A12 Diagram (test)	91.1	83.0	–	83.0
DocVQA (test)	88.4	94.5	–	93.1
VQAv2 (test)	75.2	–	81.8	77.4

baselines, achieving an average accuracy of **95.1%**. This demonstrates the effectiveness of reflection-aware fine-tuning for improving instruction alignment.

Evaluation protocol. We (i) fix evaluator prompts (see Supplementary), (ii) sample 3,000 stratified examples balanced across edit types, and (iii) compute per-evaluator agreement statistics and bootstrap confidence intervals.

General Visual Understanding

This section assesses EVLM’s ability to retain generalization across multimodal benchmarks. As summarized in Table 2, EVLM achieves strong performance despite having fewer parameters than LLAMA-11B. It attains the highest scores on MathVista (59.1) and MMMU-Pro Vision (43.8), while matching or surpassing LLAMA-11B on DocVQA (93.1) and VQAv2. These results confirm that reflection-aware training enhances alignment and reasoning quality without compromising generalization.

Cross-Dimensional Visual Editing

EVLM serves as a plug-and-play module that refines textual prompts and identifies target objects for diffusion-based editors. When integrated with IP2P (Brooks, Holynski, and Efros 2023), it outperforms both text-only (IP2P) and image-based (CSGO) approaches in precision and controllability (Fig. 4). For video editing, we apply the Tune-A-Video recipe (Wu et al. 2023), where EVLM improves temporal consistency compared with Any-V2V (Ku et al. 2024). For 3D editing, we employ 3D Gaussian Splatting (Kerbl et al. 2023) for scene reconstruction and compare against IN2N (Haque et al. 2023b) and IG2G on the IN2N and 3DEgo datasets. In 4D editing, we evaluate on DyCheck, HyperNeRF, and DyNeRF/N3DV datasets using the frameworks of (Wu et al. 2024; Mou, Chen, and Wang 2024). Across these tasks (Fig. 5), EVLM-guided edits exhibit superior spatial consistency, color coherence, and adherence to user intent.

Ablation Studies

RL Train-Set Size. We analyze the sensitivity of EVLM-RKTO to the size of the reinforcement learning (RL) training

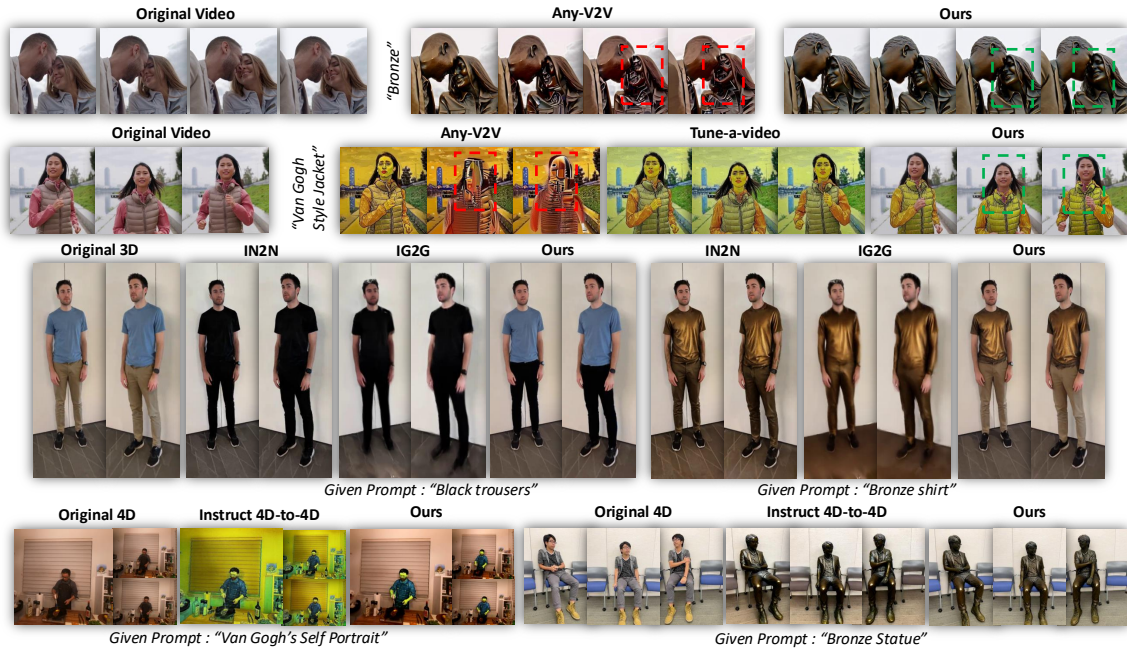


Figure 5: **Text-based editing across video, 3D, and 4D tasks.** EVLM + IP2P surpasses baselines including Any-V2V, Tune-A-Video, IN2N, and IG2G. It delivers improved style consistency (“Bronze,” “Van Gogh Style”) and stable transformations across frames.

set. Specifically, we train models on progressively smaller subsets of our original 30K dataset, using samples of 5K, 7K, and 15K. As shown in Table 3, RKTO consistently benefits from larger training data, exhibiting steady improvements in alignment and reasoning performance. Remarkably, even when trained with only 5K examples, EVLM-RKTO significantly surpasses both the base QWEN-2.5-VL-7B model and the standard EVLM-KTO variant, achieving absolute gains of 6.7% and 3.0%, respectively. These results indicate that incorporating self-reflection within RL training substantially enhances reasoning robustness and data efficiency, enabling strong performance even under limited supervision.

Effectiveness of Reflection-Aware RL Components. We observe that omitting any specific component of the Self-Reflection Reinforcement Learning (SRL) framework leads to performance degradation. In particular, removing the *Effectiveness Reward* (R_{eff}) results in a drop in average accuracy from 94.1% to 89.2%, indicating that the model critically depends on reward signals that explicitly evaluate the quality of reflective responses to achieve optimal reasoning. Similarly, excluding the *Reflection Reward* (R_{reflect}) reduces the

Table 3: Performance of EVLM-RKTO under varying RL train-set sizes.

Model / Components	Dataset Size	Accuracy (%)
Qwen-2.5-VL-7B	–	52.4
EVLM-KTO	5K	56.1
EVLM-RKTO	5K	59.1
EVLM-RKTO	7K	65.7
EVLM-RKTO	15K	78.2
EVLM-RKTO	30K	94.1

performance from 94.1% to 85.3%, suggesting that missing reflection steps can interfere with the model’s reasoning accuracy.

Table 4: Comparison of different training strategies evaluated by human annotators.

Method	Accuracy (%)
EVLM-KTO	75.1
EVLM-KTO (2-step thinking)	76.3
EVLM-SFT	67.2
EVLM-SFT (2-step thinking)	65.1
Ours (EVLM-RKTO)	94.1

Comparison with Alternative Training Objectives. To further validate the effectiveness of our reflection-aware fine-tuning, we train EVLM under standard KTO and SFT objectives, as well as the two-step thinking variants where the model generates `<think>...</think>` steps before generating the final editing instruction.

Table 13 summarizes the results, showing that our proposed EVLM-RKTO substantially outperforms all alternatives.

Conclusion

We present EVLM, a reflection-enabled vision–language model that resolves ambiguity in multimodal editing by combining Chain-of-Thought supervision with Reflection-aware KL-Divergence Target Optimization (RKTO). Trained on

a curated REFLECTIVE-EDIT corpus of 30,000 CoT examples and validated on 3,000 held-out cases, EVLM produces concise, disambiguated editing instructions and target masks that improve downstream diffusion- and NeRF-based editors. Empirically, RKTO improves both instruction fidelity and reflection quality, yielding strong gains across image, video, 3D, and 4D editing tasks.

Future work will (i) expand CoT diversity to capture broader user styles and edge cases, (ii) formalize R_{reflect} with additional human-in-the-loop metrics (e.g., brevity vs. usefulness trade-offs), and (iii) study statistical significance and robustness under noisy references. We believe EVLM’s reasoning-with-reflection paradigm generalizes beyond editing to other multimodal tasks that require interpretable decisions and subjective preference alignment.

References

- Bai, J.; Bai, S.; Yang, S.; Wang, S.; Tan, S.; Wang, P.; Lin, J.; Zhou, C.; and Zhou, J. 2023. Qwen-vl: A versatile vision-language model for understanding, localization, text reading, and beyond. *arXiv preprint arXiv:2308.12966*, 1(2): 3.
- Blattmann, A.; Dockhorn, T.; Kulal, S.; Mendelevitch, D.; Kilian, M.; Lorenz, D.; Levi, Y.; English, Z.; Voleti, V.; Letts, A.; et al. 2023. Stable video diffusion: Scaling latent video diffusion models to large datasets. *arXiv preprint arXiv:2311.15127*.
- Brooks, T.; Holynski, A.; and Efros, A. A. 2023. Instruct-pix2pix: Learning to follow image editing instructions. In *Proceedings of the IEEE/CVF Conference on Computer Vision and Pattern Recognition*, 18392–18402.
- Chen, X.; Lin, M.; Schärli, N.; and Zhou, D. 2024a. Teaching Large Language Models to Self-Debug. In *The Twelfth International Conference on Learning Representations*.
- Chen, Z.; Wu, J.; Wang, W.; Su, W.; Chen, G.; Xing, S.; Zhong, M.; Zhang, Q.; Zhu, X.; Lu, L.; et al. 2024b. Internvl: Scaling up vision foundation models and aligning for generic visual-linguistic tasks. In *Proceedings of the IEEE/CVF Conference on Computer Vision and Pattern Recognition*, 24185–24198.
- Cheng, K.; Li, Y.; Xu, F.; Zhang, J.; Zhou, H.; and Liu, Y. 2024. Vision-Language Models Can Self-Improve Reasoning via Reflection. *arXiv preprint arXiv:2411.00855*.
- Dai, W.; Li, J.; Li, D.; Tiong, A. M. H.; Zhao, J.; Wang, W.; Li, B.; Fung, P.; and Hoi, S. 2023. InstructBLIP: Towards General-purpose Vision-Language Models with Instruction Tuning. *arXiv:2305.06500*.
- Dehghani, M.; Mustafa, B.; Djolonga, J.; Heek, J.; Minderer, M.; Caron, M.; Steiner, A.; Puigcerver, J.; Geirhos, R.; Alabdulmohsin, I. M.; et al. 2024. Patch n’pack: Navit, a vision transformer for any aspect ratio and resolution. *Advances in Neural Information Processing Systems*, 36.
- Dong, J.; and Wang, Y.-X. 2024. Vica-nerf: View-consistency-aware 3d editing of neural radiance fields. *Advances in Neural Information Processing Systems*, 36.
- Dubey, A.; Jauhri, A.; Pandey, A.; Kadian, A.; Al-Dahle, A.; Letman, A.; Mathur, A.; Schelten, A.; Yang, A.; Fan, A.; et al. 2024. The llama 3 herd of models. *arXiv preprint arXiv:2407.21783*.
- Ethayarajh, K.; Xu, W.; Muennighoff, N.; Jurafsky, D.; and Kiela, D. 2024. Kto: Model alignment as prospect theoretic optimization. *arXiv preprint arXiv:2402.01306*.
- Ge, Y.; Zhao, S.; Li, C.; Ge, Y.; and Shan, Y. 2024. SEED-Data-Edit Technical Report: A Hybrid Dataset for Instructional Image Editing. *arXiv preprint arXiv:2405.04007*.
- Haque, A.; Tancik, M.; Efros, A.; Holynski, A.; and Kanazawa, A. 2023a. Instruct-NeRF2NeRF: Editing 3D Scenes with Instructions. In *Proceedings of the IEEE/CVF International Conference on Computer Vision*.
- Haque, A.; Tancik, M.; Efros, A. A.; Holynski, A.; and Kanazawa, A. 2023b. Instruct-nerf2nerf: Editing 3d scenes with instructions. In *Proceedings of the IEEE/CVF International Conference on Computer Vision*, 19740–19750.
- Hertz, A.; Mokady, R.; Tenenbaum, J.; Aberman, K.; Pritch, Y.; and Cohen-Or, D. 2022. Prompt-to-prompt image editing with cross attention control. *arXiv preprint arXiv:2208.01626*.
- Ho, J.; Chan, W.; Saharia, C.; Whang, J.; Gao, R.; Gritsenko, A.; Kingma, D. P.; Poole, B.; Norouzi, M.; Fleet, D. J.; et al. 2022. Imagen video: High definition video generation with diffusion models. *arXiv preprint arXiv:2210.02303*.
- Huang, J.; Chen, X.; Mishra, S.; Zheng, H. S.; Yu, A. W.; Song, X.; and Zhou, D. 2023. Large language models cannot self-correct reasoning yet. *arXiv preprint arXiv:2310.01798*.
- Kamata, H.; Sakuma, Y.; Hayakawa, A.; Ishii, M.; and Narihira, T. 2023. Instruct 3D-to-3D: Text Instruction Guided 3D-to-3D conversion. *arXiv preprint arXiv:2303.15780*.
- Kawar, B.; Zada, S.; Lang, O.; Tov, O.; Chang, H.; Dekel, T.; Mosseri, I.; and Irani, M. 2023. Imagic: Text-based real image editing with diffusion models. In *Proceedings of the IEEE/CVF Conference on Computer Vision and Pattern Recognition*, 6007–6017.
- Kay, W.; Carreira, J.; Simonyan, K.; Zhang, B.; Hillier, C.; Vijayanarasimhan, S.; Viola, F.; Green, T.; Back, T.; Natsev, P.; et al. 2017. The kinetics human action video dataset. *arXiv preprint arXiv:1705.06950*.
- Kembhavi, A.; Salvato, M.; Kolve, E.; Seo, M.; Hajishirzi, H.; and Farhadi, A. 2016. A diagram is worth a dozen images. In *Computer Vision—ECCV 2016: 14th European Conference, Amsterdam, The Netherlands, October 11–14, 2016, Proceedings, Part IV 14*, 235–251. Springer.
- Kerbl, B.; Kopanas, G.; Leimkühler, T.; and Drettakis, G. 2023. 3d gaussian splatting for real-time radiance field rendering. *ACM Transactions on Graphics (ToG)*, 42(4): 1–14.
- Ku, M.; Wei, C.; Ren, W.; Yang, H.; and Chen, W. 2024. Anyv2v: A plug-and-play framework for any video-to-video editing tasks. *arXiv preprint arXiv:2403.14468*.
- Li, Y.; Yang, C.; and Ettinger, A. 2024. When Hindsight is Not 20/20: Testing Limits on Reflective Thinking in Large Language Models. In *Findings of the Association for Computational Linguistics: NAACL 2024*. Association for Computational Linguistics.

- Lin, T.-Y.; Maire, M.; Belongie, S.; Hays, J.; Perona, P.; Ramanan, D.; Dollár, P.; and Zitnick, C. L. 2014. Microsoft coco: Common objects in context. In *Computer Vision–ECCV 2014: 13th European Conference, Zurich, Switzerland, September 6–12, 2014, Proceedings, Part V 13*, 740–755. Springer.
- Liu, H.; Li, C.; Wu, Q.; and Lee, Y. J. 2024. Visual instruction tuning. *Advances in neural information processing systems*, 36.
- Lu, P.; Bansal, H.; Xia, T.; Liu, J.; Li, C.; Hajishirzi, H.; Cheng, H.; Chang, K.-W.; Galley, M.; and Gao, J. 2023. Mathvista: Evaluating mathematical reasoning of foundation models in visual contexts. *arXiv preprint arXiv:2310.02255*.
- Lu, P.; Mishra, S.; Xia, T.; Qiu, L.; Chang, K.-W.; Zhu, S.-C.; Tafjord, O.; Clark, P.; and Kalyan, A. 2022. Learn to explain: Multimodal reasoning via thought chains for science question answering. *Advances in Neural Information Processing Systems*, 35: 2507–2521.
- Madaan, A.; Tandon, N.; Gupta, P.; Hallinan, S.; Gao, L.; Wiegrefe, S.; Alon, U.; Dziri, N.; Prabhunoye, S.; Yang, Y.; et al. 2024. Self-refine: Iterative refinement with self-feedback. *Advances in Neural Information Processing Systems*, 36.
- Masry, A.; Long, D. X.; Tan, J. Q.; Joty, S.; and Hoque, E. 2022. Chartqa: A benchmark for question answering about charts with visual and logical reasoning. *arXiv preprint arXiv:2203.10244*.
- Mathew, M.; Karatzas, D.; and Jawahar, C. 2021. Docvqa: A dataset for vqa on document images. In *Proceedings of the IEEE/CVF winter conference on applications of computer vision*, 2200–2209.
- Meng, C.; Song, Y.; Song, J.; Wu, J.; Zhu, J.-Y.; and Ermon, S. 2021. Sdedit: Image synthesis and editing with stochastic differential equations. *arXiv preprint arXiv:2108.01073*.
- Mou, L.; Chen, J.-K.; and Wang, Y.-X. 2024. Instruct 4D-to-4D: Editing 4D Scenes as Pseudo-3D Scenes Using 2D Diffusion. In *Proceedings of the IEEE/CVF Conference on Computer Vision and Pattern Recognition*, 20176–20185.
- Ouali, Y.; Bulat, A.; Martinez, B.; and Tzimiropoulos, G. 2024. CLIP-DPO: Vision-Language Models as a Source of Preference for Fixing Hallucinations in LVLMS. *arXiv preprint arXiv:2408.10433*.
- Pang, R. Y.; Yuan, W.; Cho, K.; He, H.; Sukhbaatar, S.; and Weston, J. 2024. Iterative reasoning preference optimization. *arXiv preprint arXiv:2404.19733*.
- Ramesh, A.; Pavlov, M.; Goh, G.; Gray, S.; Voss, C.; Radford, A.; Chen, M.; and Sutskever, I. 2021. Zero-shot text-to-image generation. In *ICML*, 8821–8831. PMLR.
- Rombach, R.; Blattmann, A.; Lorenz, D.; Esser, P.; and Ommer, B. 2022. High-resolution image synthesis with latent diffusion models. In *CVPR*, 10684–10695.
- Ruiz, N.; Li, Y.; Jampani, V.; Pritch, Y.; Rubinstein, M.; and Aberman, K. 2023. Dreambooth: Fine tuning text-to-image diffusion models for subject-driven generation. In *Proceedings of the IEEE/CVF Conference on Computer Vision and Pattern Recognition*, 22500–22510.
- Schulman, J.; Wolski, F.; Dhariwal, P.; Radford, A.; and Klimov, O. 2017. Proximal policy optimization algorithms. *arXiv preprint arXiv:1707.06347*.
- Shao, R.; Sun, J.; Peng, C.; Zheng, Z.; Zhou, B.; Zhang, H.; and Liu, Y. 2023. Control4D: Dynamic Portrait Editing by Learning 4D GAN from 2D Diffusion-based Editor. *arXiv preprint arXiv:2305.20082*.
- Shen, E.; Singh, S.; and Kumar, B. 2023. Generative visual question answering. *arXiv preprint arXiv:2307.10405*.
- Shinn, N.; Cassano, F.; Gopinath, A.; Narasimhan, K.; and Yao, S. 2023. Reflexion: language agents with verbal reinforcement learning. In Oh, A.; Naumann, T.; Globerson, A.; Saenko, K.; Hardt, M.; and Levine, S., eds., *Advances in Neural Information Processing Systems*, volume 36, 8634–8652. Curran Associates, Inc.
- Sigurdsson, G. A.; Gupta, A.; Schmid, C.; Farhadi, A.; and Alahari, K. 2018. Charades-ego: A large-scale dataset of paired third and first person videos. *arXiv preprint arXiv:1804.09626*.
- Singer, U.; Polyak, A.; Hayes, T.; Yin, X.; An, J.; Zhang, S.; Hu, Q.; Yang, H.; Ashual, O.; Gafni, O.; Parikh, D.; Gupta, S.; and Taigman, Y. 2023. Make-A-Video: Text-to-Video Generation without Text-Video Data. In *The Eleventh International Conference on Learning Representations*.
- Sun, Z.; Shen, S.; Cao, S.; Liu, H.; Li, C.; Shen, Y.; Gan, C.; Gui, L.-Y.; Wang, Y.-X.; Yang, Y.; et al. 2023. Aligning large multimodal models with factually augmented rlhf. *arXiv preprint arXiv:2309.14525*.
- Sun, Z.; Yu, L.; Shen, Y.; Liu, W.; Yang, Y.; Welleck, S.; and Gan, C. 2024. Easy-to-hard generalization: Scalable alignment beyond human supervision. *arXiv preprint arXiv:2403.09472*.
- Tumanyan, N.; Geyer, M.; Bagon, S.; and Dekel, T. 2022. Plug-and-Play Diffusion Features for Text-Driven Image-to-Image Translation. *arXiv preprint arXiv:2211.12572*.
- Wang, K.; Pan, J.; Shi, W.; Lu, Z.; Zhan, M.; and Li, H. 2024a. Measuring multimodal mathematical reasoning with math-vision dataset. *arXiv preprint arXiv:2402.14804*.
- Wang, P.; Bai, S.; Tan, S.; Wang, S.; Fan, Z.; Bai, J.; Chen, K.; Liu, X.; Wang, J.; Ge, W.; et al. 2024b. Qwen2-vl: Enhancing vision-language model’s perception of the world at any resolution. *arXiv preprint arXiv:2409.12191*.
- Wang, W.; Lv, Q.; Yu, W.; Hong, W.; Qi, J.; Wang, Y.; Ji, J.; Yang, Z.; Zhao, L.; Song, X.; Xu, J.; Xu, B.; Li, J.; Dong, Y.; Ding, M.; and Tang, J. 2023. CogVLM: Visual Expert for Pretrained Language Models. *arXiv:2311.03079*.
- Weng, Y.; Zhu, M.; Xia, F.; Li, B.; He, S.; Liu, S.; Sun, B.; Liu, K.; and Zhao, J. 2023. Large Language Models are Better Reasoners with Self-Verification. In *The 2023 Conference on Empirical Methods in Natural Language Processing*.
- Wu, G.; Yi, T.; Fang, J.; Xie, L.; Zhang, X.; Wei, W.; Liu, W.; Tian, Q.; and Wang, X. 2024. 4d gaussian splatting for real-time dynamic scene rendering. In *Proceedings of the IEEE/CVF Conference on Computer Vision and Pattern Recognition*, 20310–20320.

Wu, J. Z.; Ge, Y.; Wang, X.; Lei, S. W.; Gu, Y.; Shi, Y.; Hsu, W.; Shan, Y.; Qie, X.; and Shou, M. Z. 2023. Tune-a-video: One-shot tuning of image diffusion models for text-to-video generation. In *Proceedings of the IEEE/CVF International Conference on Computer Vision*, 7623–7633.

Xu, G.; Jin, P.; Hao, L.; Song, Y.; Sun, L.; and Yuan, L. 2024. LLaVA-o1: Let Vision Language Models Reason Step-by-Step. *arXiv preprint arXiv:2411.10440*.

Yang, Z.; Teng, J.; Zheng, W.; Ding, M.; Huang, S.; Xu, J.; Yang, Y.; Hong, W.; Zhang, X.; Feng, G.; et al. 2024. Cogvideox: Text-to-video diffusion models with an expert transformer. *arXiv preprint arXiv:2408.06072*.

Ye, Q.; Xu, H.; Xu, G.; Ye, J.; Yan, M.; Zhou, Y.; Wang, J.; Hu, A.; Shi, P.; Shi, Y.; et al. 2023. mplug-owl: Modularization empowers large language models with multimodality. *arXiv preprint arXiv:2304.14178*.

Ye, Q.; Xu, H.; Ye, J.; Yan, M.; Hu, A.; Liu, H.; Qian, Q.; Zhang, J.; and Huang, F. 2024. mPLUG-Owl2: Revolutionizing Multi-modal Large Language Model with Modality Collaboration. In *2024 IEEE/CVF Conference on Computer Vision and Pattern Recognition (CVPR)*, 13040–13051. IEEE.

Yu, T.; Zhang, H.; Yao, Y.; Dang, Y.; Chen, D.; Lu, X.; Cui, G.; He, T.; Liu, Z.; Chua, T.-S.; et al. 2024. Rlaif-v: Aligning mllms through open-source ai feedback for super gpt-4v trustworthiness. *arXiv preprint arXiv:2405.17220*.

Yue, X.; Ni, Y.; Zhang, K.; Zheng, T.; Liu, R.; Zhang, G.; Stevens, S.; Jiang, D.; Ren, W.; Sun, Y.; et al. 2024. Mmmu: A massive multi-discipline multimodal understanding and reasoning benchmark for expert agi. In *Proceedings of the IEEE/CVF Conference on Computer Vision and Pattern Recognition*, 9556–9567.

Zhang, L.; and Agrawala, M. 2023. Adding Conditional Control to Text-to-Image Diffusion Models. *arXiv preprint arXiv:2302.05543*.

Zhang, L.; Hu, A.; Xu, H.; Yan, M.; Xu, Y.; Jin, Q.; Zhang, J.; and Huang, F. 2024. Tinychart: Efficient chart understanding with visual token merging and program-of-thoughts learning. *arXiv preprint arXiv:2404.16635*.

Zhao, H.; Ma, X.; Chen, L.; Si, S.; Wu, R.; An, K.; Yu, P.; Zhang, M.; Li, Q.; and Chang, B. 2024. UltraEdit: Instruction-based Fine-Grained Image Editing at Scale. *arXiv preprint arXiv:2407.05282*.

Zhou, D.; Wang, W.; Yan, H.; Lv, W.; Zhu, Y.; and Feng, J. 2022. MagicVideo: Efficient Video Generation With Latent Diffusion Models. *arXiv preprint arXiv:2211.11018*.

Zhu, D.; Chen, J.; Shen, X.; Li, X.; and Elhoseiny, M. 2023. Minigt-4: Enhancing vision-language understanding with advanced large language models. *arXiv preprint arXiv:2304.10592*.

Zhuang, J.; Wang, C.; Lin, L.; Liu, L.; and Li, G. 2023. Dreameditor: Text-driven 3d scene editing with neural fields. In *SIGGRAPH Asia 2023 Conference Papers*, 1–10.

A Overview

Following is the content list of the supplementary material.

- Sec. B: EVLM training Algorithm (SFT ↔ RKTO).
- Sec. C: Evaluation Details..
- Sec. D: Evaluation statistics.
- Sec. E: Theoretical Analysis.
- Sec. F: Implementation Details.
- Sec. G: Dataset generation, prompts, and distributions.
- Sec. H: Additional Results.
- Sec. I: Ablation Studies.
- Sec. J: User Study
- Sec. K: Limitations.

B Training Algorithm

Algorithm 1 summarizes the iterative training procedure: initial Supervised Fine-Tuning (SFT) to learn structured CoT traces, followed by alternating RKTO optimization to align outputs and reflections with human preferences.

Algorithm 1 Iterative Training with SFT and RKTO

Require: Reference input R , Original input O , Dataset $\mathcal{D} = \{(x_i, y_i^{\text{ref}}, r_i^{\text{ref}})\}$, SFT epochs E_{SFT} , RKTO epochs E_{RKTO}

- 1: Initialize EVLM model ρ_ϕ from Qwen2-VL-7B backbone
- 2: **for** $e = 1$ **to** E_{SFT} **do**
- 3: Minimize $\mathcal{L}_{\text{SFT}} = -\sum_t \log p_\phi(y_t^{\text{ref}} | y_{<t}, x)$
- 4: Periodically save SFT snapshot ρ_{ref}
- 5: **end for**
- 6: **for** $e = 1$ **to** E_{RKTO} **do**
- 7: Sample preference batch $\{(x_i, y_{\text{pref}}^{(i)}, R_{\text{eff}}^{(i)}, R_{\text{reflect}}^{(i)})\}$
- 8: Compute importance weights and $\hat{\mathcal{L}}_{\text{RKTO}}$ (Eq. 9)
- 9: Update ϕ using the estimator in Eq. 12 (policy-gradient + reflection surrogate)
- 10: **if** checkpoint time **then** save $\rho_{\text{ref}} \leftarrow \rho_\phi$
- 11: **end if**
- 12: **end for**

Implementation notes:

- We cache SFT log-probs to reduce RKTO computation where possible.
- RKTO uses a smaller LR than SFT for stability (see Sec. F).
- Non-differentiable components (IoU) are optimized using REINFORCE with baseline centering.

C Evaluation Details

This section reproduces the evaluator prompts and a concise summary of human annotator instructions used in the experiments (these were fixed for the 3,000-example evaluation split).

LLM evaluator prompt

You are given: (1) the original image (and reference image/text if present), (2) a human reference editing instruction,

and (3) an automatically generated editing instruction. Your task: answer YES if the generated instruction semantically matches the human reference (i.e., would produce a visually similar edit to the target), otherwise answer NO. Consider object identity, target region, and transformation details. Do not hallucinate details beyond the provided inputs. Reply with a single token: YES or NO.

Human annotator instructions

Annotators received the following guidelines (full guideline documents were provided to raters and released with code):

- Present the original image, the reference (if any), and the candidate instruction side-by-side.
- Ask: “Does this instruction, when applied, match the intended edit?” — answer YES/NO.
- Provide illustrative examples of YES and NO cases, emphasizing object semantics (“bag”, “jacket”), region specificity (“left sleeve”), and transformation type (“change color”, “add pattern”).
- Ambiguous cases: use majority vote among 3 raters; record per-rater judgments to compute Cohen’s and Fleiss’ kappa.
- Instruct annotators not to assume external context beyond the shown reference(s).

D Evaluation Statistics

We describe the protocol used to compute per-evaluator accuracies, bootstrap confidence intervals (CIs), and inter-rater agreement reported in the paper.

Evaluation sampling

- Draw a stratified evaluation set of $N = 3,000$ examples balanced across edit types (color, style, texture, object-replacement, layout change).
- For each example, collect binary judgments (YES/NO) from each evaluator (LLMs and humans).

Bootstrap CI computation

1. Draw 10,000 bootstrap resamples (with replacement) of size N from the evaluation set.
2. For each resample and each evaluator, compute the fraction of YES responses.
3. The reported 95% CI is the empirical 2.5th–97.5th percentile of the bootstrap distribution.

Agreement measures

- For human annotators, compute pairwise Cohen’s κ and Fleiss’ κ when groups of 2 raters are used.
- For human vs. LLM agreement, compute percent agreement and Cohen’s κ between LLM judgments and the majority human label.

Representative CI numbers (example)

Table 5 reproduces the representative bootstrap statistics included in the supplement (replace with final numbers upon camera-ready).

Table 5: Representative bootstrap statistics for EVLM-RKTO.

Evaluator	Mean Accuracy (%)	95% Bootstrap CI (%)
Gemini Pro 1.5	95.4	[94.2, 96.4]
LLAMA 405B	94.8	[93.5, 95.9]
GPT-4o	96.2	[95.1, 97.3]
Claude 3.5 Sonnet	95.1	[93.9, 96.2]
Human (majority)	94.1	[92.8, 95.4]
Average (EVLM-RKTO)	95.1	[94.0, 96.0]

E Theoretical Analysis

E.1 Notation and Batched RKTO Objective

Here we restate the key symbols and provide the batched empirical form of the RKTO objective used during training.

- $x = (\mathcal{V}, u)$: multimodal input context, consisting of visual inputs \mathcal{V} and textual prompt u . \mathcal{V} may include an RGB image, video clip, depth map, or OCR-extracted text.
- \hat{y} : model-generated instruction tokens; \hat{m} : predicted mask (decoded from mask tokens, when available); m_{ref} : reference mask.
- $\rho_\phi(\cdot | x)$: current model (EVLM) conditional distribution, parameterized by ϕ .
- $\rho_{\text{ref}}(\cdot | x)$: reference policy (the SFT snapshot baseline).
- $\rho_{\text{pref}}(\cdot | x)$: empirical human-preferred distribution.
- y_{pref} : human-preferred response corresponding to input x .
- $R_{\text{eff}} \in [0, 1]$: instruction-effectiveness reward (semantic + mask IoU).
- $R_{\text{reflect}} \in [0, 1]$: reflection-quality reward.
- $w(\cdot)$: monotonic importance-weight function, defined as $w(s) = \text{clip}(\text{softplus}(s), 0, w_{\text{max}})$ with $\text{softplus}(s) = \log(1 + e^s)$.
- $\lambda_{\text{ref}} \geq 0$: weighting coefficient for reflection alignment.
- $e(\cdot)$: Qwen2-VL text encoder embedding function; cosine values are rescaled to $[0, 1]$ via $\widetilde{\text{cos}}(a, b) = (1 + \cos(a, b))/2$.
- Intersection-over-Union (IoU) between predicted and reference masks:

$$\text{IoU}(\hat{m}, m_{\text{ref}}) = \frac{|\hat{m} \cap m_{\text{ref}}|}{|\hat{m} \cup m_{\text{ref}}|}.$$

For a mini-batch $\{(x_i, y_{\text{pref}}^{(i)})\}_{i=1}^B$, the normalized log-ratio statistics are computed as:

$$\hat{s}_\phi^{(i)} = \log \frac{\rho_\phi(y_{\text{pref}}^{(i)} | x_i)}{\rho_{\text{ref}}(y_{\text{pref}}^{(i)} | x_i)}, \quad (7)$$

$$\hat{\eta}_0 = \max\left(0, \frac{1}{B(B-1)} \sum_{i \neq j} \log \frac{\rho_\phi(y_{\text{pref}}^{(j)} | x_i)}{\rho_{\text{ref}}(y_{\text{pref}}^{(j)} | x_i)}\right). \quad (8)$$

The empirical RKTO loss minimized during training is

$$\widehat{\mathcal{L}}_{\text{RKTO}} = \frac{1}{B} \sum_{i=1}^B \left[w(\hat{s}_\phi^{(i)} - \hat{\eta}_0) R_{\text{eff}}^{(i)} + \lambda_{\text{ref}} R_{\text{reflect}}^{(i)} \right]. \quad (9)$$

E.2 Instruction Effectiveness R_{eff}

The instruction-effectiveness reward $R_{\text{eff}} \in [0, 1]$ measures how well the generated instruction \hat{y} matches the human reference y_{pref} both semantically and spatially. It combines:

1. the cosine similarity between text embeddings of \hat{y} and y_{pref} , rescaled to $[0, 1]$; and
2. the Intersection-over-Union (IoU) between predicted and reference masks, also normalized.

The final convex combination is

$$R_{\text{eff}} = \alpha \widetilde{\text{cos}}(e(\hat{y}), e(y_{\text{pref}})) + (1 - \alpha) \text{IoU}(\hat{m}, m_{\text{ref}}), \quad (10)$$

where α is tuned on a validation set ($\alpha=0.7$ in our experiments).

E.3 Reflection Reward R_{reflect}

The reflection-quality reward encourages concise, semantically consistent self-reflection. We employ the differentiable surrogate:

$$R_{\text{reflect}} = \beta_1 \widetilde{\text{cos}}(e(r_{\text{ref}}), e(y_{\text{pref}})) + \beta_2 \exp(-\gamma \text{len}(r_{\text{ref}})) + \beta_3 (1 - \text{KL}(p_{\text{int}} \| p_{\text{ref}})), \quad (11)$$

where:

- r_{ref} : reflection segment from the model’s CoT trace;
- $p_{\text{int}}, p_{\text{ref}}$: token distributions for the `<intermediate>` and `<reflection>` segments;
- $\text{len}(\cdot)$: token length of reflection (brevity term);
- coefficients $\beta_1 + \beta_2 + \beta_3 = 1$ with $\beta_k \geq 0$.

The differentiable reflection loss is $\mathcal{L}_{\text{reflect}} = 1 - R_{\text{reflect}}$. For non-differentiable components of R_{eff} (e.g., IoU), we apply REINFORCE with a batch-mean baseline (see Sec. E.4).

E.4 Gradient Estimator and Variance Reduction

Differentiating Eq. (9) yields the gradient estimator used in training. For compactness, define $c_i = w(\hat{s}_\phi^{(i)} - \hat{\eta}_0)$ and $d_i = c_i (1 - \alpha) (\text{IoU}^{(i)} - b_{\text{IoU}})$. Then

$$\begin{aligned} \nabla_\phi \widehat{\mathcal{L}}_{\text{RKTO}} \approx & \frac{1}{B} \sum_{i=1}^B c_i R_{\text{eff}}^{(i)} \nabla_\phi \log \rho_\phi(y_{\text{pref}}^{(i)} | x_i) \\ & + \lambda_{\text{ref}} \nabla_\phi \mathcal{L}_{\text{reflect}} \\ & + \frac{1}{B} \sum_{i=1}^B d_i \nabla_\phi \log \rho_\phi(\hat{m}^{(i)} | x_i). \end{aligned} \quad (12)$$

Variance reduction techniques include: (i) clipping $w(\cdot)$ to $[0, w_{\text{max}}]$; (ii) centering rewards ($R - \bar{R}$); (iii) smaller learning rate for RKTO ($\text{LR}_{\text{RKTO}} \ll \text{LR}_{\text{SFT}}$); (iv) averaging multiple Monte-Carlo mask samples per example; and (v) gradient and importance-weight clipping.

E.5 Expected-KL Improvement

The following theorem formalizes the expected improvement guarantee of the RKTO surrogate.

Table 6: Data Distribution for EVLM CoT Fine-Tuning

Reference	Original	# of Samples
Image	Image	10,000
Image+Text	Image	5,000
Video	Image	4,000
Image	Video	3,000
Video+Text	Image	3,000
Text	-	5,000

Theorem 1 (Monotonic Alignment Guarantee). *Let rewards R_{ref} and R_{reflect} be bounded in $[0, 1]$, $w(\cdot)$ be non-decreasing and bounded, and training steps sufficiently small. Define*

$$\mathcal{K}(\phi) = \text{KL}(\rho_\phi(y | x) \parallel \rho_{\text{pref}}(y | x)) + \lambda_{\text{ref}} \text{KL}(\rho_\phi(r_{\text{ref}} | x) \parallel \rho_{\text{pref}}(r_{\text{ref}} | x)). \quad (13)$$

Then any update step that decreases $\mathcal{L}_{\text{RKTO}}$ in expectation also decreases $\mathbb{E}_x[\mathcal{K}(\phi)]$, ensuring joint alignment of output and reflection distributions.

Proof. The gradient of each KL term can be expressed, via the log-derivative trick, as an expectation of $\nabla_\phi \log \rho_\phi$ weighted by the log-density ratio. The RKTO objective employs the same log-ratio statistic s_ϕ with baseline η_0 and monotonic weight $w(\cdot)$. Because the rewards are bounded and w preserves ordering, the update direction of $-\nabla_\phi \mathcal{L}_{\text{RKTO}}$ is aligned with that of $\nabla_\phi \mathcal{K}(\phi)$ in expectation. Therefore, sufficiently small gradient steps that reduce $\mathcal{L}_{\text{RKTO}}$ also reduce the expected composite divergence $\mathcal{K}(\phi)$, guaranteeing monotonic improvement. \square

F Implementation Details

Representative defaults used in experiments:

- Optimizer: AdamW. SFT LR = 5×10^{-5} ; RKTO LR = 2×10^{-5} .
- Batch size $B = 64$ (use gradient accumulation if needed).
- $\lambda_{\text{ref}} = 0.2$, $\beta = (0.5, 0.2, 0.3)$, $\gamma = 0.2$.
- $w_{\text{max}} = 10$, softplus threshold $\tau = 0.1$.
- Monte-Carlo samples per example: 3 (empirical trade-off between variance and cost).
- Reference policy ρ_{ref} : SFT snapshot (pre-compute/caching of log-probs when feasible).
- LoRA rank 64, alpha 16, dropout 0.05 (when LoRA used).

Compute usage (approx):

- SFT (30k samples): ~ 48 GPU-hours on $8 \times \text{A100}$ (80GB).
- RKTO stage: ~ 36 GPU-hours on $8 \times \text{A100}$ (80GB).

G Dataset details and prompts

To train EVLM for multimodal editing instruction generation, we developed a comprehensive dataset that emphasizes diversity in input modalities and output clarity. The dataset preparation process involved **generation**, **augmentation**, and **refinement with human evaluation**, ensuring both the quality and breadth of data. In our training, we also include nearly 20% training samples from cross-domain datasets used in

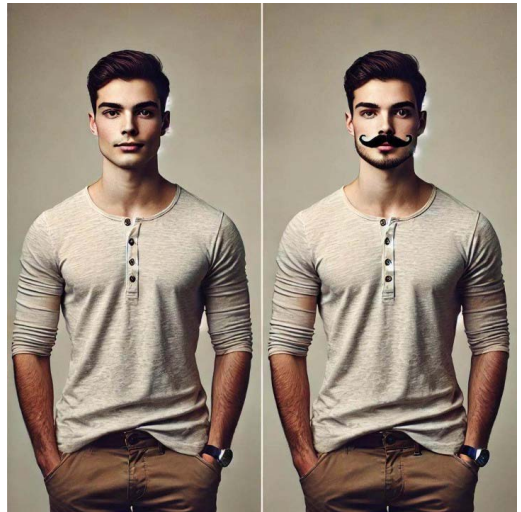


Figure 6: An example of a diptych generated for the EVLM dataset using DALL-E-3. The left panel displays the original image, while the right panel showcases the edited image, reflecting the instruction to add a mustache.

(Cheng et al. 2024; Chen et al. 2024b; Xu et al. 2024) in addition to our MME data. Cross-benchmark evaluations in the main paper use:

- MMMU / MMMU-Pro (Yue et al. 2024)
- MathVista (Lu et al. 2023)
- ChartQA (Masry et al. 2022)
- AI2 Diagram (Kembhavi et al. 2016)
- DocVQA (Mathew, Karatzas, and Jawahar 2021)
- VQA_{v2} (Shen, Singh, and Kumar 2023)

Dataset Overview The dataset consists of 30,000 samples distributed across six categories of input combinations, as shown in Table 6. Each sample contains:

- **Reference Input (R):** A combination of image, video, or text to provide editing context.
- **Original Input (O):** The target image or video requiring modifications.
- **Reflective Rationale and Instruction:** A detailed rationale generated by GPT-4o, followed by a human-reviewed editing instruction.

Generation of Paired Images To prepare a subset where both the reference and the original are images, we generate paired image samples using DALL-E 3. Since we want EVLM to understand the relationship between the given reference and original visual cues, instead of relying solely on textual descriptions, we create **diptychs**, where the original input image and the edited output image are displayed side by side. This approach enhances alignment and correspondence between input-output image pairs by ensuring both visual and semantic consistency.

We use prompts designed to capture various transformations while maintaining the visual integrity of the input image.

Table 7: Examples of Reference Images and Corresponding Editing Instructions

Reference Image 1	Reference Image 2	Editing Instruction
Einstein’s face	Green threads	Turn his face into Einstein and turn his jacket green.
Batman’s face	Blue shirt	Turn his face into Batman and turn his shirt blue.
Spider-Man’s mask	Leather jacket	Turn his face into Spider-Man’s mask and turn his jacket into leather.
Mona Lisa’s face	Green dress	Turn her face into Mona Lisa’s face and turn her dress green.
Robotic face	Black boots	Turn his face into a robotic face and turn his boots black.
Cat’s face	Yellow scarf	Turn their face into a cat’s face and turn their scarf yellow.
Superman’s face	Red trousers	Turn his face into Superman’s face and turn his trousers red.
A clown’s face	Striped T-shirt	Turn his face into a clown’s face and turn his T-shirt into a striped pattern.
Iron Man’s mask	Metallic armor	Turn his face into Iron Man’s mask and turn his outfit into metallic armor.
A Viking’s face	Fur coat	Turn his face into a Viking’s face and turn his coat into fur.
A painter’s face	Multi-colored apron	Turn her face into a painter’s face and turn her apron multi-colored.
Santa Claus’s face	Red and white suit	Turn his face into Santa Claus and turn his outfit into a red and white suit.
A robot’s head	Silver gloves	Turn his face into a robot’s head and turn his gloves silver.
A pirate’s face	Black hat	Turn his face into a pirate’s face and add a black hat.
A magician’s face	White gloves	Turn his face into a magician’s face and turn his gloves white.
A superhero’s face	Cape	Turn his face into a superhero’s face and add a red cape.
A lion’s face	Golden mane	Turn their face into a lion’s face and turn their hairstyle into a golden mane.
A wizard’s face	Magic staff	Turn his face into a wizard’s face and add a magic staff to his hand.
A medieval knight’s face	Shiny armor	Turn his face into a medieval knight’s face and turn his outfit into shiny armor.

For instance, to generate the paired image from DALL-E 3 shown in Figure 6, we use a prompt like:

Generate a diptych with two side-by-side images. On the left side, there should be a person standing confidently with a neutral expression, wearing casual clothing. On the right side, show the same person with a mustache while keeping the rest of the visual attributes unchanged.

This methodology allows for generating a variety of image pairs that focus on specific edits, such as adding or removing objects, changing facial features, or modifying global attributes like color or style. By leveraging DALL-E 3’s generative capabilities, we ensure that the resulting diptychs are coherent and contextually aligned, providing a strong foundation for fine-tuning EVLM.

Figure 6 illustrates an example of such a diptych. The left panel represents the reference image, while the right panel reflects the transformation specified by the prompt. This technique is particularly effective when working with samples where textual input is minimal or absent, as it allows EVLM to focus on interpreting visual relationships directly. We have furnished some examples in Table where we use two reference images.

Overall, the diptych approach not only simplifies the editing process but also improves the model’s understanding of contextual relationships between the original and modified visual content. By avoiding dependency on detailed textual descriptions, this method provides a streamlined and efficient pathway for multimodal image editing.

In addition to using DALL-E 3 for generating paired images, we further leverage Stable Diffusion XL to create

Table 8: Examples of Ambiguous Text and Image as References for Editing Instructions

Reference 1 (Text)	Reference 2 (Image)	Editing Instruction
Make it heroic	Superman’s costume	Turn his outfit into Superman’s costume while keeping his face unchanged.
Give it a metallic vibe	A shiny silver texture	Turn the jacket into a silver metallic style while preserving the rest of the image.
Bring a touch of royalty	A golden crown	Add a golden crown to the person’s head without altering their facial features.
Add an artistic feel	Van Gogh’s painting	Turn his jacket into a style resembling Van Gogh’s Starry Night painting.
Transform into a character	Spider-Man’s suit	Change his outfit into Spider-Man’s suit while leaving his face intact.
Make it winter-ready	A fur coat	Replace his jacket with a warm fur coat suitable for winter.
Add a festive spirit	Christmas decorations	Turn her dress into a Christmas-themed outfit with red and white patterns.
Create a futuristic look	A robotic arm design	Replace his arms with robotic prosthetics while keeping the rest of the image unaltered.
Make it classic	A vintage tuxedo	Turn his outfit into a vintage tuxedo, keeping his hairstyle and face the same.
Turn it into nature	A green leafy texture	Change her jacket into a pattern resembling green leaves.
Add a magical touch	A wizard’s robe	Transform his outfit into a wizard’s robe with stars and moons.
Show some adventure	A pirate’s hat	Add a pirate’s hat and an eyepatch while leaving the outfit unchanged.
Brighten it up	A vibrant yellow scarf	Add a yellow scarf to her outfit without altering any other details.
Make it sporty	A football jersey	Replace his shirt with a football jersey representing a famous team.
Bring a cultural touch	A traditional Japanese kimono	Turn her outfit into a traditional Japanese kimono.

a diverse set of high-quality image samples. These generated images undergo pre-processing to ensure compatibility and are combined with other open-source datasets such as IN2N, 3DEgo, DyNeRF, and MSCOCO (Lin et al. 2014) to form reference-original pairs. This combination enriches the dataset with varied visual transformations and styles, enhancing the robustness of EVLM. For video-based pairs, we employ generative video models like CogVideoX-5B (Yang et al. 2024) and Stable Video Diffusion (Blattmann et al. 2023) to synthesize reference videos, while the original videos are sourced from publicly available datasets, including Kinetics (Kay et al. 2017) and Charades (Sigurdsson et al. 2018). This multi-source, multi-modality data preparation process ensures that the training data encapsulates a wide range of visual edits and transformations, providing EVLM with the capability to generalize across diverse scenarios.

Reference Text. Figure 9 illustrates the distribution of instruction (Reference Text) lengths given as an input to EVLM. 8000/30000 samples have the reference text in addition to reference image or a video. EVLM’s instructions, typically ranging from 1–4 words, demonstrate the model’s ability to perform complex editing tasks with minimal and concise textual input, unlike InstructPix2Pix, which relies on more detailed instructions exceeding 4 words. Figure 10 provides

a detailed view of the types of edits and their frequency, showcasing the dataset’s balanced coverage of diverse editing tasks. We additionally created samples incorporating both textual and visual references, as illustrated in Table 8.

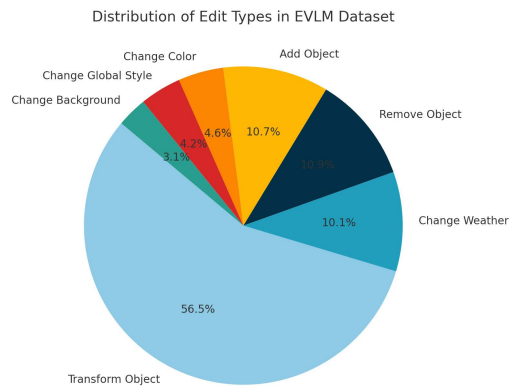


Figure 10: Distribution of Edit Types in the EVLM Dataset. The dataset covers diverse editing tasks, with the majority focusing on object transformations.

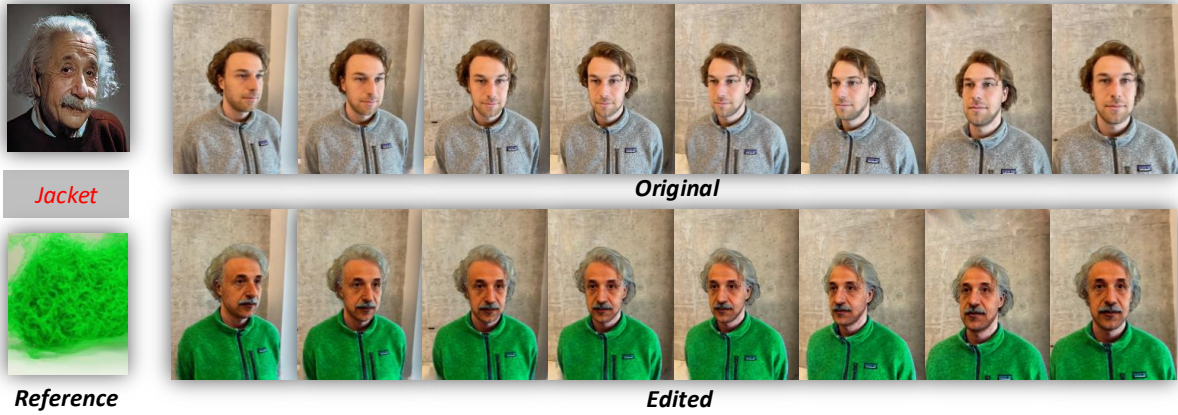


Figure 7: **Reference Image and Text.** Examples of 3D editing results generated using EVLM + IP2P. The model produces context-aware editing instructions based on the reference content, autonomously interpreting the editing rationale to generate optimal instructions for the desired outcome. This example demonstrates multi-attribute editing, where the jacket is transformed into green, and the face is altered to resemble Einstein.

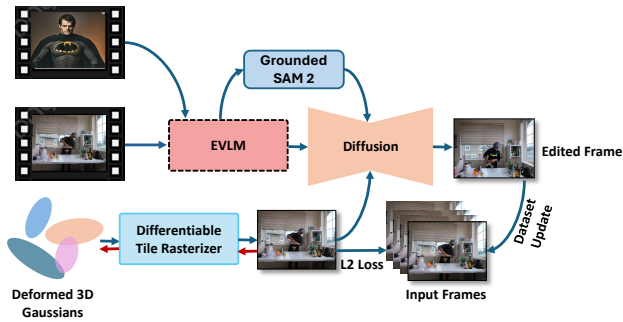


Figure 8: The 4D editing pipeline guided by EVLM, which outputs both the editing instruction and the target object to be modified. The identified target object is passed through Grounded SAM 2 to generate precise masks, which guide local editing in the diffusion model based on the provided instruction. The edited frames are then iteratively updated in the dataset to ensure temporal and spatial consistency, while an L2 loss is applied between input and edited frames for quality refinement, resulting in a consistent and temporally smooth 4D dataset.

Data Quality Assessment To ensure high data quality, the dataset underwent the following refinements:

- **Human Evaluation:** Human raters validated and refined GPT-4o-generated rationales and instructions to align with subjective editing preferences.
- **Instruction Clarity:** Editing instructions were enriched to include sufficient detail, distinguishing them from the vague instructions typically used in baseline models.
- **Balanced Task Representation:** The dataset was carefully curated to balance global edits (e.g., changing weather or background) and local edits (e.g., object transformation or removal), as illustrated in Figure 10.

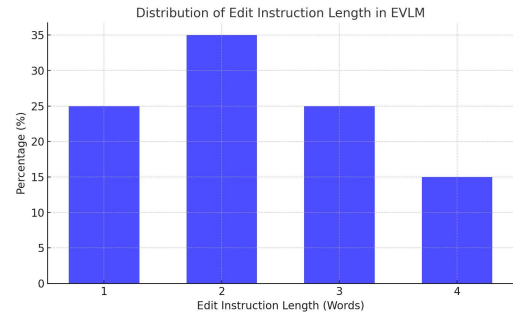


Figure 9: EVLM effectively performs editing tasks using concise instructions (1–4 words), whereas InstructPix2Pix requires longer and more detailed instructions (4 or more words).

Edit Diversity The dataset spans a wide range of editing tasks, encompassing both global and local transformations. As shown in Figure 10, the majority of tasks involve object transformations (56.5%), followed by weather changes (10.1%), object removals (10.9%), and object additions (10.7%). The diversity of edit types ensures that EVLM can generalize across varied scenarios.

By integrating reflective reasoning, human evaluation, and diverse multimodal inputs, this dataset provides a robust foundation for training EVLM to generate accurate and human-aligned editing instructions.

H Additional Results

The figure 8 demonstrates how EVLM processes the reference video and original video to generate context-aware editing instructions and execute the desired transformations. In this specific 4D editing example, the goal is to change the person’s clothing into a Batman costume while preserving

the face, as the reference video does not depict a Batman face. EVLM interprets the required editing from the reference and original videos, outputs the object label (clothing), and passes it to Grounded-SAM, which generates precise masks for the targeted region. These masks ensure that only the clothing is affected during the editing process. The editing instruction is then fed into a diffusion model, which applies the required transformation to the clothing while maintaining the integrity of other visual attributes, such as the face. The edited frames are iteratively replaced in the original dataset, creating a modified dataset aligned with the desired edits. Training is continued on this edited dataset to refine the alignment of deformed 3D Gaussians with the edited frames, ensuring the model’s enhanced capacity to generalize and align with complex transformations.

For 3D editing, we do not utilize deformed Gaussians; instead, we employ the standard Gaussian Splatting technique (Kerbl et al. 2023). Along with this supplementary document, we have provided the rendered videos for both 4D-editing and 3D-editing. Additionally, Figure 7 showcases a 3D editing example where the input to EVLM consists of four components: two images (Einstein and green threads), one text prompt (jacket), and multiple frames of a person’s face. The model autonomously interprets the editing intent and generates the instruction: *Turn his face into Einstein and turn his jacket into green.* This instruction can then be utilized with (Brooks, Holynski, and Efros 2023) to perform the desired edits, as illustrated in the Figure 7.

I Ablation Studies

We analyze the sensitivity of EVLM to its main hyperparameters.

I.1 Effect of reflection weight λ_{ref}

As shown in Table 9, increasing λ_{ref} strengthens reflective reasoning until $\lambda_{\text{ref}} > 0.2$, where excessive emphasis on reflection marginally reduces instruction fidelity.

Table 9: Ablation on λ_{ref} .

λ_{ref}	Accuracy (%)	Reflection Q	IoU
0.00	88.0	0.62	0.41
0.05	90.5	0.68	0.46
0.10	92.3	0.72	0.51
0.20	94.1	0.78	0.58
0.50	93.4	0.80	0.56

I.2 Importance-weight cap w_{max}

Smaller caps stabilize training but slow convergence; larger caps risk variance spikes. Table 10 shows $w_{\text{max}}=10$ achieves the best trade-off.

Table 10: Ablation on w_{max} .

w_{max}	Accuracy (%)	Comment
5	92.1	conservative weighting
10	94.1	default, stable
20	93.6	slightly higher variance

Table 11: Ablation on MC samples for importance-weight estimation.

MC samples	Accuracy (%)	Runtime \times factor
1	92.8	1.0
2	93.9	1.3
3	94.1	1.6 (default)
4	94.2	2.0
8	94.3	3.8

Table 12: Surrogate vs REINFORCE for reflection reward.

Method	Accuracy (%)	Note
Surrogate-only	93.8	lower variance
Surrogate + REINFORCE (IoU)	94.1	best overall
REINFORCE-only	92.9	unstable

I.3 Monte-Carlo samples per example

Table 11 shows that three samples strike an effective balance between accuracy and runtime.

I.4 Reflection reward formulation

Replacing the differentiable surrogate with REINFORCE increases variance and slows convergence. Combining both retains stability while preserving gradient signal for mask IoU (Table 12).

I.5 Alternative objectives

We further compared pure SFT, KTO, and RKTO (Table 13). Results confirm that reflection-aware optimization yields the strongest alignment.

Table 13: Training-objective comparison (human evaluation).

Method	Accuracy (%)
EVLM-KTO	75.1
EVLM-KTO (2-step thinking)	76.3
EVLM-SFT	67.2
EVLM-SFT (2-step thinking)	65.1
EVLM-RKTO	94.1

Discussion. Across all ablations, the reflection weight λ_{ref} and surrogate-based reflection reward have the largest impact. Moderate reflection emphasis (0.2) ensures coherent reasoning without over-regularizing the generation policy.

RKTO thus balances reasoning depth and instruction fidelity, producing interpretable and precise edits.

Table 14: Contextual alignment from user study.

Editing Type	EVLM	Best Baseline
2D Editing	4.82	IP2P: 4.32
Video Editing	4.77	Tune-A-Video: 4.41
3D Editing	4.65	IN2N: 4.38
4D Editing	4.58	Instruct 4D-to-4D: 4.42

J User study

To evaluate the contextual alignment of EVLM compared to other methods, we conducted a user study involving 50 participants aged between 20 and 40. Each participant evaluated the contextual alignment of editing outputs on a scale of 1 to 5 across four editing types: 2D, video, 3D, and 4D editing. Participants were presented with pairs of reference inputs (text, images, or videos) and their corresponding edited outputs and were tasked with rating how well the edits aligned with the intended context. The study involved a total of 200 edits, with 50 edits per task, and 20 randomly selected edits were assigned to each participant for evaluation.

The Table 14 presents the average scores across all users for each method. EVLM consistently outperformed competing methods (IP2P for 2D editing, TAV for video editing, IN2N for 3D editing, and Instruct 4D-to-4D for 4D editing) across all editing types. However, no method achieved a perfect 5.0 score, reflecting the subjective nature of the task and variability in user preferences. The results demonstrate EVLM’s superior ability to understand and apply contextual cues, particularly in complex multimodal scenarios like 3D and 4D editing.

K Limitations

While EVLM demonstrates significant advancements in generating context-aware editing instructions, it has several limitations. The model heavily relies on the quality and diversity of its training dataset, which, despite comprising 30,000 samples, may not generalize well to highly complex or unseen scenarios. Its dependency on human-rated rationales introduces subjectivity, and its computationally intensive reflective reasoning framework and KL-Divergence Target Optimization (KTO) limit scalability for large-scale or real-time applications. Furthermore, EVLM struggles with ambiguous textual references and conflicting multimodal inputs, and it primarily supports object-specific edits, making it less effective for global scene-level transformations. The precision of mask generation by Grounded-SAM impacts the quality of detailed edits, and the lack of dynamic or incremental training reduces adaptability to new styles or user preferences. Additionally, EVLM is restricted to text and vision modalities, excluding other forms of input such as audio, which limits its applicability in broader multimodal contexts. These limitations provide opportunities for future improvements in dataset diversity, scalability, and multimodal adaptability.